

Electron Tesla valve

Daniil I. Sarypov,^{1,2,*} Dmitriy A. Pokhabov,^{1,2} Arthur G. Pogosov,^{1,2}
Evgeny Yu. Zhdanov,^{1,2} Andrey A. Shevyrin,¹ and Askhat K. Bakarov^{1,2}

¹*Rzhanov Institute of Semiconductor Physics SB RAS, Novosibirsk, 630090, Russia*

²*Novosibirsk State University, Novosibirsk, 630090, Russia*

In solids, frequent electron-electron collisions can induce collective, fluid-like electron transport. While this regime offers a powerful framework for exploring many-body phenomena, there is still a lack in functional electronic device actively exploiting hydrodynamic behaviour of electrons. Here, we introduce a solid-state analogue of a Tesla valve — a passive fluidic diode that rectifies flow without moving parts. Lithographically defined in high-mobility GaAs two-dimensional electron gas, the device exhibits abrupt rectification producing a more than tenfold difference between forward and reverse resistances. This threshold behaviour, reminiscent of the onset of turbulence in fluidic Tesla valves, points to the emergence of turbulent regime in the electron liquid — a long-predicted, but yet unobserved state of electronic matter. More broadly, our work demonstrates the fruitfulness of the hydrodynamic analogy: fluidic technologies can be readily adopted to create novel electronic devices. Here, this is realized through a solid-state rectifier whose operation relies on a new physical mechanism, interparticle collisions.

In conventional theories of electron transport in solids, electrical resistance is governed by momentum-relaxing scattering processes: interactions with impurities, defects and phonons. Electron-electron (e - e) collisions, although frequent, are typically considered secondary because they conserve total momentum of the electron system and therefore do not directly contribute to resistivity. In sufficiently clean conductors, however, e - e collisions can dominate the charge carrier dynamics, and electron system behaves as a collective medium whose motion can be described within a hydrodynamic framework [1, 2]. Recent experiments have confirmed this picture, revealing many-body phenomena characteristic of viscous fluids, including Poiseuille electron flow in microchannels [3–5], current vortices [6–8] and superballistic transport [9–14].

The hydrodynamic analogy between electron liquids and classical fluids has thus proven remarkably fruitful, offering intuitive insight into collective phenomena and suggesting new routes for engineering interaction-dominated transport. Yet an important question remains: how far can this analogy be extended? In particular, can it encompass highly nonlinear phenomena such as turbulence, one of the central problems of fluid dynamics?

A natural way to address this question is to transpose well-known fluidic devices into electronic systems and test whether they operate similarly. An especially intriguing can-

didate is Tesla valve — a fixed-geometry passive valve that allows fluid to flow more easily in one direction than the other, without any moving parts. Its design consists of a series of interconnected, teardrop-shaped loops [Fig. 1a]. Patented over a century ago [15], it remains actively studied for its complex internal flow physics [16–18] and potential applications in heat transfer [19, 20]. The next logical step is to merge hydrodynamic behaviour of electrons in solids with unique properties of Tesla valve by exploring electron transport in structures that mimic its fluidic counterparts. Beyond fundamental interest, an electronic analogue of fluidic Tesla valve could be a promising candidate for THz applications among other geometric diodes [21]. However, the concept of an “electron Tesla valve” is almost unexplored: the only study in graphene reports [22] a vanishing rectification of $\sim 5\%$, which is intriguing but far from capturing the full depth of the Tesla valve behaviour.

In this work, we introduce the electron Tesla valve created from GaAs [Figs. 1b,c] — a material where the fluid-like behaviour of electrons is widely reported [11, 23–30]. Faithful to Tesla’s original geometry [15], the devices consist of multiple loops and exhibit strong rectification, with reverse resistance exceeding forward resistance by more than an order of magnitude [Fig. 1d]. Notably, the rectification features closely mirrors those of turbulent fluidic Tesla valve [18], while achieved diodicity values substantially higher than those reported in classical fluidic devices—pointing to the emergence of a turbulent regime in the electron liquid. These findings underscore the universality of hydrodynamic description: the

* d.sarypov@g.nsu.ru

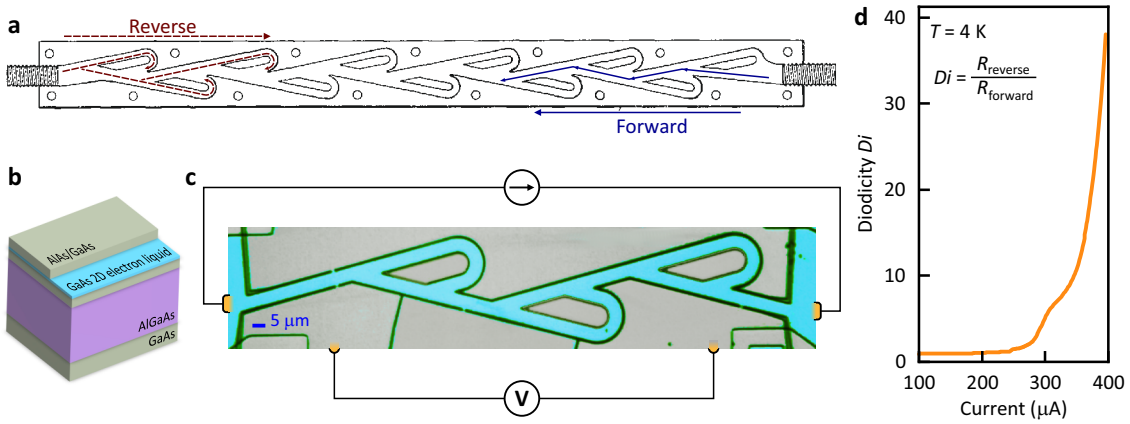


Figure 1: GaAs Tesla valve for electron liquid. **a**, Schematics of original design adopted from N. Tesla’s patent [15]. **b**, GaAs/AlGaAs heterostructure with two-dimensional electron liquid in a GaAs quantum well. **c**, False-color optical micrograph of one of the created valves, overlaid with the four-probe measurement schematic. Scale bar is $5 \mu\text{m}$. **d**, Diode efficiency Di for device shown in **b**, measured as the ratio of reverse to forward resistance values.

Tesla valve operation relies on the same physical mechanism whether it is driven by water or an electron liquid. Beyond fundamental insights into non-Ohmic electron dynamics, they open pathways toward functional hydrodynamic electronic components.

GaAs Tesla valves. The devices are fabricated on the basis of GaAs/AlGaAs heterostructures with high-mobility two-dimensional electron gas (2DEG) [Fig. 1b, Extended data Fig. 1a]. At $T = 4 \text{ K}$, 2DEG has a density of $n = 6.8 \times 10^{11} \text{ cm}^{-2}$, determined from Shubnikov-de Haas oscillations [Extended data Figs. 1b-d], and mobility $\mu \approx 10^6 \text{ cm}^2/(\text{V}\cdot\text{s})$, measured in macroscopic samples made of the same heterostructure (see “Methods”). Driving the electron system into the hydrodynamic regime requires frequent e - e collisions, which is achieved by raising the temperature of electron system — either by heating the lattice (increasing the sample temperature) or by passing a DC current [23]. On the other hand, raising the temperature intensifies electron-phonon scattering, which breaks momentum conservation, i.e. hydrodynamic regime, and restores conventional Ohmic transport. For high-mobility 2DEG in GaAs quantum wells, this leaves a window below approximately 40 K [24, 25, 30] where e - e collisions are frequent but electron-phonon scattering is still negligible allowing hydrodynamic effects to be clearly resolved. Building on these conditions, we performed transport measurements in the extended temperature range of 4–70 K and DC current up $\sim 10^{-3} \text{ A}$.

The Tesla valves are patterned by electron lithography in the plane of a 2DEG, with characteristic channel width W of 2.5 and $5 \mu\text{m}$, where the wider valve is scaled proportionally

from narrower one [Fig. 2a]. Micron-scaled width of the samples supports hydrodynamic transport while excluding ballistic mechanisms responsible for rectification in so-called “ballistic rectifiers” [31–33]. Those devices rely on the collimation or reflection of narrow electron beams and therefore require submicron dimensions. These conditions do not apply to the valves studied here.

In fluidic systems, the rectification of Tesla valves turns on at high enough Reynolds numbers $Re > 1$ [18, 34–36], corresponding to high flow rates. Here, we follow the approach of Ref. [18], where the rectification is captured by measuring fluid flow rate as function of pressure drop across the device, and measure current-voltage (I - V) characteristics of the valves across a wide range of electric current [Fig. 2b]. In forward direction, where electrons bypass the internal loops [Fig. 1a], the I - V curve in narrow and wide samples resembles that of a straight macroscopic channel: linear at low bias and saturating at high voltages. The saturation current in both valves corresponds to the same current density of $j = I/W \approx 260 \text{ A/m}$, i.e. the same drift velocity of $v_d = j/(ne) \approx 2 \times 10^5 \text{ m/s}$. This value is close to the maximal drift velocity reported for electrons in GaAs quantum wells [37–39], indicating that the I - V flattening in forward flow direction is due to the drift velocity saturation in studied GaAs structures.

Surprisingly, the electron flow in the reverse direction behaves qualitatively differently [Fig. 2b]. Below $I \approx 300 \mu\text{A}$, the I - V curves coincide with those corresponding to forward bias, but, at higher currents, they sharply diverge, and electron transport becomes direction-dependent. Notably, lower reverse saturation currents along with the overall shape of the

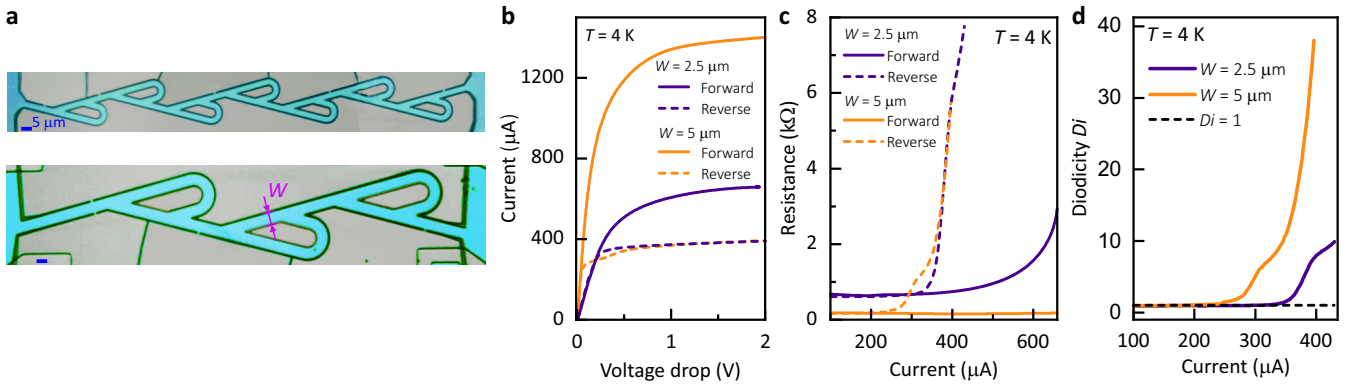


Figure 2: Electron transport in Tesla valves. **a**, False-color optical micrograph of GaAs Tesla valves of different widths. **b**, I - V characteristics of the devices shown in **a** at lattice temperature of $T = 4$ K. **c,d** Resistance of Tesla valves and diodicity Di as functions of DC current at lattice temperature of $T = 4$ K.

I - V curves points on current-limiting physical mechanism distinct from the drift velocity saturation.

Rectification effect. The features of direction-dependent transport are clearly resolved in [Fig. 2c] that shows the resistance of the valves $R = V/I$ as function of DC current. Namely, as reverse current exceeds the value of 250–350 μA , we observe sharp increase of the resistance while the forward resistance remains low (< 1 k Ω) and almost unchanged indicating linear transport [Fig. 2a]. To quantify this behaviour and test the performance of the valves, we evaluate the diodicity Di , which is a standard characteristics of asymmetric resistors defined as the ratio of reverse to forward resistance values [18, 40]:

$$Di = \frac{R_{\text{reverse}}}{R_{\text{forward}}}.$$

Accordingly, the valve rectifies the flow if $Di > 1$. In the studied valves, rectification emerges abruptly and the diodicity rising steeply to values as high as $Di \approx 40$ in wider valve [Fig. 2d]. An important feature of the diodicity curves is a plateau. A similar structure is also observed in fluidic Tesla valves [18] where sharp threshold of diodicity followed by the plateau is attributed to the onset of turbulence. The Di plateau can be a signature of transition process. For water flow in a Tesla valve, such a plateau corresponds to the progressive filling of the structure with intermixed turbulent flows as Re number increases [18]. Once the valve is fully saturated with turbulence, the transition concludes and diodicity continues to grow. The studied electron liquid appears to exhibit the same behaviour: the diodicity curve in the electron Tesla valve qualitatively reproduces that of its fluidic analogue. This close sim-

ilarity points to the universal rectification mechanism in both fluidic and electronic Tesla valves — the turbulence of hydrodynamic flow.

Such a scenario is plausible since the geometry of the Tesla valve itself favours head-on interparticle collisions, which shifts the onset of turbulence to lower Reynolds numbers Re [18]. In electron systems, Re can be large enough, especially at a high DC current that drives the system deeper into hydrodynamic regime by raising electron temperature with respect to the lattice [23]. Our estimates give a Reynolds number $Re \gtrsim 7$ at $I \gtrsim 350$ μA (see “Methods” section for details), which is well above unity. Earlier simulations [41, 42] predict the onset of electron turbulence at higher $Re \gtrsim 20$ in flow past circular obstacle. We note, however, that the critical Reynolds number is highly sensitive to device geometry. In a Tesla valve, with its characteristic looped shape, the emergence of turbulence is expected at substantially lower Re values, which is confirmed in water-flow experiments [18]. Our estimates therefore support the interpretation that turbulent dynamics underlies the observed rectification in electron Tesla valves.

To test the robustness of the rectification, we measured the diodicity at various lattice temperatures [Fig. 3a]. As the temperature increases from 4 to ≈ 20 K, the diodicity plateau smoothly weakens while the curves remain almost converged at $Di > 10$. Further, at $T \gtrsim 20$ K, the diodicity is significantly suppressed until rectification is almost vanished at $T = 70$ K. This suppression can be explained by growing influence of electron-phonon scattering, which disrupts the collective flow and, thus, the rectification effect. The strength of this scattering is quantified by the momentum relaxing length l_{MR} , which we measure independently in a macroscopic Hall bar made of the same heterostructure as Tesla valves (Fig. 3b,

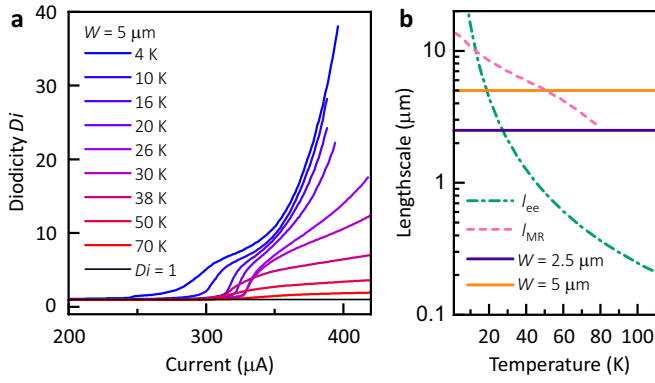


Figure 3: Temperature dependence of the diodicity. **a**, Diodicity Di of wide ($W = 5 \mu\text{m}$) Tesla valve at different lattice temperatures. **b**, Characteristic lengthscales of studied system: widths W of the Tesla valves, momentum relaxing length l_{MR} , e - e scattering length l_{ee} .

"Methods"). Below $T < 20 \text{ K}$, l_{MR} exceeds $10 \mu\text{m}$, which is well above the Tesla valve width W , meaning that electrons rarely lose their momentum on phonons, and diodicity remains high. Above $T > 20 \text{ K}$, l_{MR} becomes comparable to or smaller than W , showing increased electron-phonon scattering rate, that leads to expected suppression of diodicity. Notably, e - e scattering remains frequent even at low lattice temperature due to high DC current which heats electron system [23, 29]. At $I = 350 \mu\text{A}$, we estimate electron temperature $T_e \approx 100 \text{ K}$ (see "Methods"), where e - e scattering length drops below $0.5 \mu\text{m}$, ten times lower than W [Fig. 3b]. This ensures that e - e collisions are abundant reinforcing the many-body origin of the rectification.

Finally, to isolate the features of electron transport in Tesla valves, we fabricated the reference devices with $W \approx 2 \mu\text{m}$ that reproduce the geometry of the main channel in Tesla valves but contain no loops [Fig. 4]. As expected, their I - V characteristics are symmetric and similar to that of Tesla valve under forward bias [Fig. 1d]. This confirms that the observed rectification arises solely from the Tesla valve geometry, whose looped design promotes head-on e - e collisions leading to large reverse resistance.

Together, our findings reveal that the hydrodynamic description transcends classical fluids: a rectification mechanism reported in fluidic Tesla valves [18] operates equally in its electronic analogue. The asymmetric geometry places the created devices in the class of geometric diodes, yet the electron Tesla valve demonstrates remarkably high performance, with a diode efficiency Di up to 40, which is several times greater than the typical $Di \lesssim 2$ reported for other geometric rectifiers [43, 44]. Their planar structure yields low intrinsic capacitance, a natural advantage for high-frequency opera-

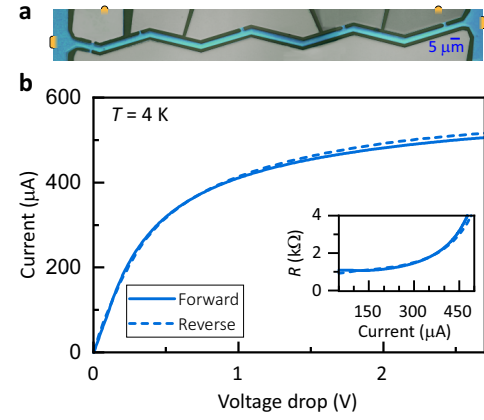


Figure 4: No rectification in a reference sample without loops. **a**, False-color optical image of the reference device. **b**, I - V characteristics of the device demonstrating no rectification. Inset shows the resistance of the reference sample as function of DC current.

tion [21]. These results open a path towards exploring electron Tesla valves at terahertz frequencies, where their performance could be benchmarked against existing high-speed rectifiers [32, 33].

ACKNOWLEDGMENTS

The study was funded by the Russian Science Foundation (Grant No. 22-12-00343-II).

AUTHORS CONTRIBUTIONS

D.I.S. and D.A.P. suggested, carried the project and analyzed the experimental data. D.A.P. and A.G.P. supervised the project. D.I.S. performed measurements with the technical support of E.Yu.Z. A.A.S. and A.K.B. fabricated samples. D.I.S. and D.A.P. wrote the manuscript. D.A.P., A.G.P. and A.A.S. contributed to the discussion.

METHODS

A. Growth of heterostructure.

The GaAs/AlGaAs heterostructure, the basis of our samples, is grown in following steps: growth of $\text{Al}_{0.8}\text{Ga}_{0.2}\text{As}$ layer (400 nm thick) on GaAs (001) substrate, growth of the heterostructure (160 nm thick) consisting of GaAs/AlAs superlattice, which is alternating layers of GaAs (2.3 nm thick) and AlAs (1.15 nm thick), and GaAs quantum well for electrons

(13 nm thick). The structure was doped by Si δ -layers with a density of $1.5 \times 10^{12} \text{ cm}^{-2}$ located at a distance of 40 nm on both sides of the quantum well. The growth process is summarized in Extended Data Figure 1a.

B. Lithography

Large areas, including ohmic contacts, and the reference samples [Fig. 4] are patterned with photolithography and subsequent wet etching. Electron beam lithography was used to create the Tesla valves. To form the device boundaries, reactive ion etching is then performed through resist mask.

C. Transport measurements

Experimental samples are equipped with the Au/Ge/Ni ohmic contacts. Electrical measurements are performed in a dry VTI cryostat (Oxford Instruments Teslatron PT system) using 4-probe scheme, as shown in Fig. 1c, to exclude lead resistance. To measure Shubnikov-de Haas oscillations in Tesla valve [Extended data Figs. 1 b-d], we used lock-in technique at the frequency of 70 Hz and the excitation current amplitude of 100 nA.

D. Characteristics of electron system: scattering lengths, electron temperature and Reynolds number.

Momentum-relaxing length is extracted from the electron mobility measured in macroscopic Hall bar fabricated from the same GaAs/AlGaAs heterostructure as the Tesla valves.

The Hall bar has a length and width of $L = 50 \mu\text{m}$ and $W = 20 \mu\text{m}$, respectively [Extended data Fig. 1e]. The mobility μ is converted from the Hall bar resistance R as $\mu = 1/(neR) \times L/W$. Both values are shown in Extended data Figs. 1 f,g. Then, the momentum-relaxing length l_{MR} is obtained from the mobility as $l_{\text{MR}} = mv_F \mu / e$ (m , v_F are effective electron mass in GaAs and Fermi velocity, respectively).

Electron-electron scattering length, shown in [Fig. 2d], is calculated using the well-known formula of Giuliani and Quinn [45]:

$$l_{ee} = \frac{4\pi}{k_F} \left(\frac{E_F}{k_B T} \right)^2 \left[\ln \left(\frac{E_F}{k_B T} \right) + \ln \left(\frac{2q_{TF}}{k_F} \right) + 1 \right]^{-1}.$$

Here, $E_F = \pi \hbar^2 n / m = 24 \text{ meV}$ is Fermi energy, $k_F = \sqrt{2mE_F} / \hbar \approx 2.07 \times 10^8 \text{ m}^{-1}$ is Fermi wavenumber, $q_{TF} = 2me^2 / (\hbar^2 \epsilon_{\text{GaAs}}) \approx 2 \times 10^8 \text{ m}^{-1}$ is inverse screening length for a 2DEG. This expression is confirmed [30, 46] to accurately describe e - e scattering in studied 2DEG in GaAs quantum wells.

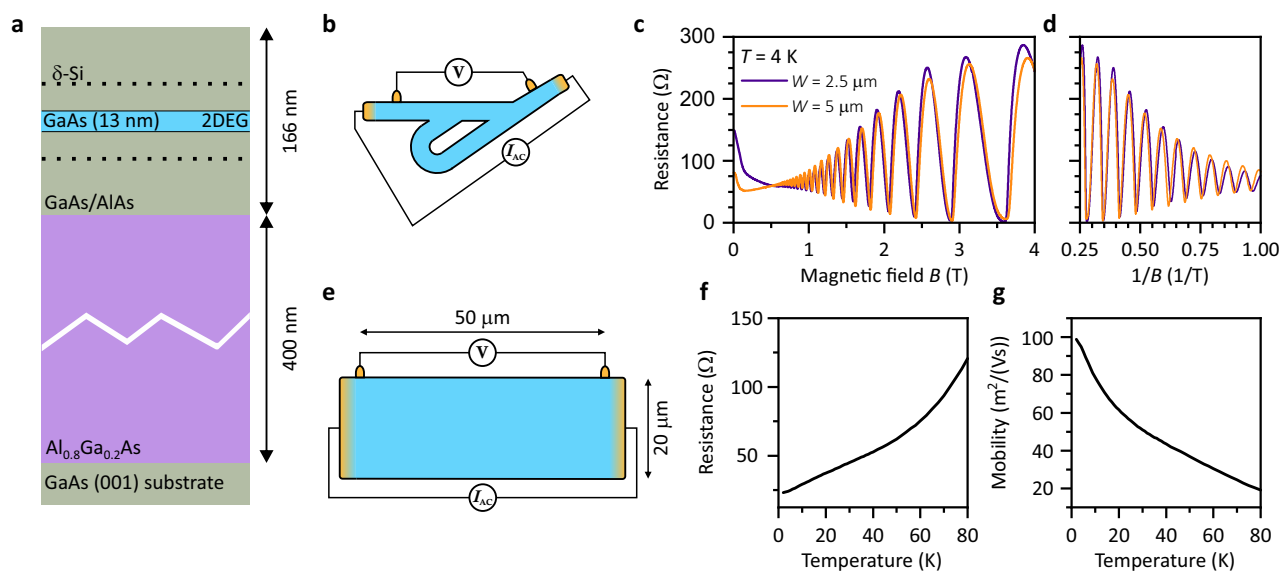
To estimate the values of electron temperature T_e and Reynolds number Re in our samples, we use the known energy-loss rates for electrons in GaAs quantum well [47]. At $I \approx 350 \mu\text{A}$, power input from electric field is $P \approx I \cdot V \approx 350 \mu\text{W}$ [Fig. 1d] yielding energy-loss rate per particle of $P/(nS) \approx 2 \times 10^{-10} \text{ W}$ ($S \approx 1 \times 100 \mu\text{m}^2$ is the estimated area of the valve), which corresponds to $T_e \approx 100 \text{ K}$ [47]. At this temperature, viscosity of electron liquid can be lower than $\nu \approx 6 \times 10^{-2} \text{ m}^2/\text{s}$ [14], giving a Reynolds number

$$Re = \frac{v_d W}{\nu} \equiv \frac{I}{nev} \gtrsim 7.$$

-
- [1] R. N. Gurzhi, Hydrodynamic effects in solids at low temperature, *Sov. Phys. Usp.* **11**, 255 (1968).
- [2] L. Fritz and T. Scaffidi, Hydrodynamic Electronic Transport, *Annu. Rev. Condens. Matter Phys.* **15**, 17 (2024).
- [3] J. A. Sulpizio, L. Ella, A. Rozen, J. Birkbeck, D. J. Perello, D. Dutta, M. Ben-Shalom, T. Taniguchi, K. Watanabe, T. Holder, R. Queiroz, A. Principi, A. Stern, T. Scaffidi, A. K. Geim, and S. Ilani, Visualizing Poiseuille flow of hydrodynamic electrons, *Nature* **576**, 75 (2019).
- [4] M. J. H. Ku, T. X. Zhou, Q. Li, Y. J. Shin, J. K. Shi, C. Burch, L. E. Anderson, A. T. Pierce, Y. Xie, A. Hamo, U. Vool, H. Zhang, F. Casola, T. Taniguchi, K. Watanabe, M. M. Fogler, P. Kim, A. Yacoby, and R. L. Walsworth, Imaging viscous flow of the Dirac fluid in graphene, *Nature* **583**, 537 (2020).
- [5] U. Vool, A. Hamo, G. Varnavides, Y. Wang, T. X. Zhou, N. Kumar, Y. Dovzhenko, Z. Qiu, C. A. C. Garcia, A. T. Pierce, J. Gooth, P. Anikeeva, C. Felser, P. Narang, and A. Yacoby, Imaging phonon-mediated hydrodynamic flow in WTe₂, *Nat. Phys.* **17**, 1216 (2021).
- [6] D. A. Bandurin, I. Torre, R. K. Kumar, M. Ben Shalom, A. Tomadin, A. Principi, G. H. Auton, E. Khestanova, K. S. Novoselov, I. V. Grigorieva, L. A. Ponomarenko, A. K. Geim, and M. Polini, Negative local resistance caused by viscous electron backflow in graphene, *Science* **351**, 1055 (2016).
- [7] A. Aharon-Steinberg, T. Völkl, A. Kaplan, A. K. Pariari, I. Roy, T. Holder, Y. Wolf, A. Y. Meltzer, Y. Myasoedov, M. E. Huber, B. Yan, G. Falkovich, L. S. Levitov, M. Hücker, and E. Zeldov, Direct observation of vortices in an electron fluid, *Nature* **607**, 74

- (2022).
- [8] M. L. Palm, C. Ding, W. S. Huxter, T. Taniguchi, K. Watanabe, and C. L. Degen, Observation of current whirlpools in graphene at room temperature, *Science* **384**, 465 (2024).
- [9] H. Guo, E. Ilseven, G. Falkovich, and L. S. Levitov, Higher-than-ballistic conduction of viscous electron flows, *Proc. Natl. Acad. Sci.* **114**, 3068 (2017).
- [10] R. Krishna Kumar, D. A. Bandurin, F. M. D. Pellegrino, Y. Cao, A. Principi, H. Guo, G. H. Auton, M. Ben Shalom, L. A. Ponomarenko, G. Falkovich, K. Watanabe, T. Taniguchi, I. V. Grigorieva, L. S. Levitov, M. Polini, and A. K. Geim, Superballistic flow of viscous electron fluid through graphene constrictions, *Nature Phys* **13**, 1182 (2017).
- [11] L. V. Ginzburg, C. Gold, M. P. Rössli, C. Reichl, M. Berl, W. Wegscheider, T. Ihn, and K. Ensslin, Superballistic electron flow through a point contact in a Ga[Al]As heterostructure, *Phys. Rev. Res.* **3**, 023033 (2021).
- [12] M. Kravtsov, A. L. Shilov, Y. Yang, T. Pryadilin, M. A. Kashchenko, O. Popova, M. Titova, D. Voropaev, Y. Wang, K. Shein, I. Gayduchenko, G. N. Goltzman, M. Lukianov, A. Kudriashov, T. Taniguchi, K. Watanabe, D. A. Svintsov, S. Adam, K. S. Novoselov, A. Principi, and D. A. Bandurin, Viscous terahertz photoconductivity of hydrodynamic electrons in graphene, *Nat. Nanotechnol.* 10.1038/s41565-024-01795-y (2024).
- [13] J. Estrada-Álvarez, J. Salvador-Sánchez, A. Pérez-Rodríguez, C. Sánchez-Sánchez, V. Clericò, D. Vaquero, K. Watanabe, T. Taniguchi, E. Diez, F. Domínguez-Adame, M. Amado, and E. Díaz, Superballistic Conduction in Hydrodynamic Antidot Graphene Superlattices, *Physical Review X* **15**, 011039 (2025).
- [14] D. I. Sarypov, D. A. Pokhabov, A. G. Pogosov, E. Y. Zhdanov, A. A. Shevyrin, A. K. Bakarov, and A. A. Shklyaev, Temperature Dependence of Electron Viscosity in Superballistic GaAs Point Contacts, *Phys. Rev. Lett.* **134**, 026302 (2025).
- [15] N. Tesla, Valvular conduit (1920), U.S. Patent 1,329,559.
- [16] P. R. Porwal, S. M. Thompson, D. K. Walters, and T. Jamal, Heat transfer and fluid flow characteristics in multistaged Tesla valves, *Numerical Heat Transfer, Part A: Applications* **73**, 347 (2018).
- [17] J. Raffel, S. Ansari, and D. S. Nobes, An Experimental Investigation of Flow Phenomena in a Multistage Micro-Tesla Valve, *Journal of Fluids Engineering* **143**, 111205 (2021).
- [18] Q. M. Nguyen, J. Abouezzi, and L. Ristroph, Early turbulence and pulsatile flows enhance diodicity of Tesla's macrofluidic valve, *Nat Commun* **12**, 2884 (2021).
- [19] W. Li, S. Yang, Y. Chen, C. Li, and Z. Wang, Tesla valves and capillary structures-activated thermal regulator, *Nature Communications* **14**, 3996 (2023).
- [20] X. Huang, R. Anufriev, L. Jalabert, K. Watanabe, T. Taniguchi, Y. Guo, Y. Ni, S. Volz, and M. Nomura, A graphite thermal Tesla valve driven by hydrodynamic phonon transport, *Nature* **634**, 1086 (2024).
- [21] H. Han, B. Zhang, P. Guo, S. Lv, Z. Cheng, Y. Li, Y. Li, Z. Zhang, and J. Zhang, Broken structural symmetry in terahertz detectors: Physical mechanisms, device design, and recent advances, *Small Structures* **6**, 2500402 (2025), <https://onlinelibrary.wiley.com/doi/pdf/10.1002/ssstr.202500402>.
- [22] J. Geurs, Y. Kim, K. Watanabe, T. Taniguchi, P. Moon, and J. H. Smet, Rectification by hydrodynamic flow in an encapsulated graphene Tesla valve (2020), arXiv:2008.04862 [cond-mat].
- [23] M. J. M. de Jong and L. W. Molenkamp, Hydrodynamic electron flow in high-mobility wires, *Phys. Rev. B* **51**, 13389 (1995).
- [24] G. M. Gusev, A. D. Levin, E. V. Levinson, and A. K. Bakarov, Viscous electron flow in mesoscopic two-dimensional electron gas, *AIP Adv.* **8**, 025318 (2018).
- [25] A. D. Levin, G. M. Gusev, E. V. Levinson, Z. D. Kvon, and A. K. Bakarov, Vorticity-induced negative nonlocal resistance in a viscous two-dimensional electron system, *Phys. Rev. B* **97**, 245308 (2018).
- [26] A. Gupta, J. J. Heremans, G. Kataria, M. Chandra, S. Fallahi, G. C. Gardner, and M. J. Manfra, Hydrodynamic and Ballistic Transport over Large Length Scales in GaAs / AlGaAs, *Phys. Rev. Lett.* **126**, 076803 (2021).
- [27] A. C. Keser, D. Q. Wang, O. Klochan, D. Y. H. Ho, O. A. Tkachenko, V. A. Tkachenko, D. Culcer, S. Adam, I. Farrer, D. A. Ritchie, O. P. Sushkov, and A. R. Hamilton, Geometric Control of Universal Hydrodynamic Flow in a Two-Dimensional Electron Fluid, *Phys. Rev. X* **11**, 031030 (2021).
- [28] X. Wang, P. Jia, R.-R. Du, L. N. Pfeiffer, K. W. Baldwin, and K. W. West, Hydrodynamic charge transport in an GaAs/AlGaAs ultrahigh-mobility two-dimensional electron gas, *Phys. Rev. B* **106**, L241302 (2022).
- [29] Z. T. Wang, M. Hilke, N. Fong, D. G. Austing, S. A. Studenikin, K. W. West, and L. N. Pfeiffer, Nonlinear transport phenomena and current-induced hydrodynamics in ultrahigh mobility two-dimensional electron gas, *Phys. Rev. B* **107**, 195406 (2023).
- [30] D. I. Sarypov, D. A. Pokhabov, A. G. Pogosov, E. Y. Zhdanov, A. A. Shevyrin, A. K. Bakarov, and A. A. Shklyaev, Slip Electron Flow in GaAs Microscale Constrictions, *Phys. Rev. Lett.* **135**, 236301 (2025).
- [31] A. M. Song, A. Lorke, A. Kriele, J. P. Kotthaus, W. Wegscheider, and M. Bichler, Nonlinear Electron Transport in an Asymmetric Microjunction: A Ballistic Rectifier, *Physical Review Letters* **80**, 3831 (1998).
- [32] G. Auton, J. Zhang, R. K. Kumar, H. Wang, X. Zhang, Q. Wang, E. Hill, and A. Song, Graphene ballistic nano-rectifier with very high responsivity, *Nat. Commun.* **7**, 11670 (2016).
- [33] G. Auton, D. B. But, J. Zhang, E. Hill, D. Coquillat, C. Consejo, P. Nouvel, W. Knap, L. Varani, F. Teppe, J. Torres, and A. Song, Terahertz Detection and Imaging Using Graphene Ballistic Rectifiers, *Nano Letters* **17**, 7015 (2017).
- [34] A. Nobakht, M. Shahsavan, and A. Paykani, Numerical Study of Diodicity Mechanism in Different Tesla-Type Microvalves, *Jour-*

- nal of Applied Research and Technology **11**, 876 (2013).
- [35] J. Kim, K.-N. Kang, Y. Jin, J. Goettert, and P. K. Ajmera, Hydrodynamic focusing micropump module with PDMS/nickel-particle composite diaphragms for microfluidic systems, *Microsystem Technologies* **21**, 65 (2015).
- [36] A. R. Gamboa, C. J. Morris, and F. K. Forster, Improvements in Fixed-Valve Micropump Performance Through Shape Optimization of Valves, *Journal of Fluids Engineering* **127**, 339 (2005).
- [37] K. Hirakawa and H. Sakaki, Hot-electron transport in selectively doped *n*-type AlGaAs/GaAs heterojunctions, *Journal of Applied Physics* **63**, 803 (1988).
- [38] N. Balkan, R. Gupta, M. Daniels, B. Ridley, and M. Emeny, Hot electron transport in GaAs quantum wells: non-drifting hot phonons, *Semiconductor Science and Technology* **5**, 986 (1990).
- [39] V. G. Mokerov, I. S. Vasil'evskii, G. B. Galiev, J. Požela, K. Požela, A. Sužiedēlis, V. Jucienė, and Č. Paškevič, Drift velocity of electrons in quantum wells in high electric fields, *Semiconductors* **43**, 458 (2009).
- [40] L. Li, J. Mo, and Z. Li, Nanofluidic diode for simple fluids without moving parts, *Phys. Rev. Lett.* **115**, 134503 (2015).
- [41] M. Mendoza, H. J. Herrmann, and S. Succi, Preturbulent Regimes in Graphene Flow, *Phys. Rev. Lett.* **106**, 156601 (2011).
- [42] R. C. V. Coelho, M. Mendoza, M. M. Doria, and H. J. Herrmann, Kelvin-Helmholtz instability of the Dirac fluid of charge carriers on graphene, *Phys. Rev. B* **96**, 184307 (2017).
- [43] V. H. Nguyen, D. C. Nguyen, S. Kumar, M. Kim, D. Kang, Y. Lee, N. Nasir, M. A. Rehman, T. P. A. Bach, J. Jung, and Y. Seo, Optimum design for the ballistic diode based on graphene field-effect transistors, *npj 2D Materials and Applications* **5**, 89 (2021).
- [44] H. Wang, M. Chen, Y. Yang, Y. Ma, L. Luo, C. Liu, I. Getmanov, T. D. Anthopoulos, X. Zhang, and A. Shamim, A Graphene Geometric Diode with the Highest Asymmetry Ratio and Three States Gate-Tunable Rectification Ability, *Adv. Electron. Mater.* **10**, 2300695 (2024).
- [45] G. F. Giuliani and J. J. Quinn, Lifetime of a quasiparticle in a two-dimensional electron gas, *Phys. Rev. B* **26**, 4421 (1982).
- [46] D. A. Egorov, D. A. Pokhobov, E. Y. Zhdanov, A. A. Shevyrin, A. K. Bakarov, and A. G. Pogosov, Enhanced e-e interaction in suspended 2DEG evidenced by transverse magnetic focusing, *Appl. Phys. Lett.* **125**, 112103 (2024).
- [47] J. Shah, A. Pinczuk, A. C. Gossard, and W. Wiegmann, Energy-Loss Rates for Hot Electrons and Holes in GaAs Quantum Wells, *Phys. Rev. Lett.* **54**, 2045 (1985).



Extended data Fig. 1: Heterostructure and transport parameters. **a**, Illustration of the GaAs/AlGaAs heterostructure. **b**, The scheme of the Tesla valve segment for magnetoresistance measurement. **c-d**, The resistance of the Tesla valve segment in magnetic field. **e**, The macroscopic Hall bar used to measure electron mobility. **f-g**, Temperature dependences of the Hall bar resistance and electron mobility.